Article

Provision of Demand-Side Flexibility through the Integration of Power-to-Gas Technologies in an Electric Steel Mill

Johannes Dock *[iD], Stefan Wallner, Anna Traupmann [iD] and Thomas Kienberger

Chair of Energy Network Technology, Department of Environmental and Energy Process Engineering, Montanuniversität Leoben, A-8700 Leoben, Austria
* Correspondence: johannes.dock@unileoben.ac.at; Tel.: +43-384-2402-5404

Abstract: EAF steelmaking based on renewable electricity allows for low-CO_2 steel production. However, the increased integration of volatile renewable energies into the energy system requires the provision of flexibility options. In view of the substantial oxygen consumption in the steel mill, flexible on-site generation and storage holds a significant potential for demand-side management. The utilization of by-product oxygen from an electrolysis plant not only contributes to load flexibility but also generates a climate-neutral fuel. In the present study, different process layouts are developed based on state-of-the-art technologies. The proposed supply systems for oxygen, hydrogen, and synthetic natural gas are subjected to design and operational optimization and assessed with respect to the overall demand-side flexibility, carbon dioxide emission reduction, and economic viability.

Keywords: EAF steelmaking; demand-side management; oxygen production; pressure swing adsorption; electrolysis; res integration; climate neutrality

1. Introduction

In view of the climate neutrality of the steel industry, steel production via the electric arc furnace (EAF) has certain advantages over the conventional blast furnace/basic oxygen furnace (BF/BOF) route. First, the reduction of iron ore using coke in the blast furnace is associated with substantial energy consumption and carbon dioxide emissions. The recycling of steel scrap, referred to as secondary production, in the EAF omits the entire reduction process step. With regard to steel production from iron ore (primary production), the processing of direct reduced iron (DRI) in the EAF offers a viable and lower-emission alternative. Consequently, EAF steelmaking plays a key role in numerous future technology scenarios in addition to carbon capture, utilization, and storage (CCUS) and smelting reduction [1–4].

Second, the EAF route is characterized by a high degree of electrification. The Greenhouse Gas Protocol defines three scopes for greenhouse gas accounting [5]. According to this definition, in the EAF steel mill, direct (scope 1) CO_2 emissions occur mainly in energy-intensive by-processes such as ladle heating, annealing, and steam generation [6]. In contrast, indirect (scope 2) carbon dioxide emissions of the production process depend solely on the CO_2 intensity of the supplied electric energy. The operation of the electric arc furnace with electricity that is certified as 100% climate neutral thus eliminates scope 2 emissions and, therefore, represents an effective emission reduction measure. However, increased integration of volatile renewable energy sources (RES) into the energy system requires flexibility options to balance both temporal and spatial fluctuations [7] and to reduce the strain on the grid infrastructure [8].

1.1. EAF Steel Production Process and Oxygen Demand

The remelting of steel scrap in the EAF is not only the most energy-intensive process step in electric steelmaking [9] but also causes significant oxygen consumption: During the

melting phase, chemical energy input by the introduction of oxygen, carbon, and natural gas reduces the electric energy demand and tap-to-tap time. The following refining step aims at dephosphorization, decarburization, and temperature adjustment of the steel melt. In order to protect the furnace lining, the slag is foamed by the injection of carbon and oxygen through lances [10]. For the production of stainless steel, decarburization is carried out in a separate argon oxygen decarburization (AOD) or vacuum oxygen decarburization (VOD) process to inhibit the oxidation of valuable alloying elements. Both the AOD and the VOD process involve the injection of oxygen [10]. Due to the high consumption in the steel mill, we identified the flexible oxygen production from electrical energy as a promising demand-side management option.

Further process steps, which are referred to as secondary metallurgy, include de-oxidation, desulfurization, degassing, homogenization, alloying, and temperature and composition adjustment [11]. Subsequently, the steel is casted either continuously or in ingots. Throughout secondary steelmaking, steel mill ladles are used as a transport and processing vessel. Prior to tapping of the steel melt at the electric arc furnace, they have to be preheated to more than 1000 °C. In a preceding study, the authors demonstrated that the application of Oxyfuel burners for ladle preheating rather than natural gas/air burners results in significant energy savings [6]. In Oxyfuel combustion, natural gas is burnt with oxygen, which leads to higher combustion efficiency but increases the oxygen demand in the steel mill.

1.2. Technology Overview

In the following section, we will discuss options for demand-side management in steel mills and the flexible operation of oxygen production and power-to-gas (PtG) plants.

1.2.1. Demand-Side Management in EAF Steel Mills

An efficient way to provide flexibility to the power system is to apply demand-side management (DSM). DSM describes the concept of matching the demand with the available supply, encouraging the customers in the energy market to actively manage their energy consumption [12]. Consumer-end measures include either reducing the energy consumption or shifting the energy demand to a later time [13]. According to Strbac [14], the implementation of DSM measures has the potential to reduce the generating margin, improve the operation efficiency of transmission and distribution grids, and facilitate the integration of intermittent renewable energy sources into existing energy systems.

Due to the batch operation, high nominal power, and substantial energy consumption, many studies focus on the electric arc furnace. Flexible scheduling of an EAF allows for the shifting of high power [15]. However, deferring the production schedule of the EAF impairs the subsequent processes such as secondary metallurgy and casting, degrades the asset utilization rate, and decreases the steel production volume. Zhang and Grossmann [16] give an overview of the challenges and benefits of industrial DSM. They conclude that exploiting the synergies of interdependent production processes holds potential for demand-side management. Coupling a steel mill with an oxygen production plant might serve this purpose. Another DSM option is the implementation of power-to-gas (PtG) plants that produce climate-neutral gases such as hydrogen and synthetic natural gas (SNG) from fluctuating renewable electricity [17].

1.2.2. Oxygen Production

Oxygen has the potential to enhance the efficiency of energy-intensive industrial processes such as glass melting, pulp bleaching, and iron, steel, and non-ferrous metal production [18]. Therefore, considerable research effort has been dedicated to its energy- and cost-efficient production. At present, two processes are commercially available for the industrial-scale production of oxygen: For the large-volume production of oxygen with high purity, cryogenic air separation (ASU) constitutes the standard process [19]. Pressure swing adsorption (PSA) offers an alternative for the production at lower throughputs [20].

The customizable plant capacity and the controllable operation of the PSA allow for the flexible on-site production of oxygen [21]. Depending on the purity, capacity, physical state and output pressure, manufacturer data for specific energy consumption ranges from 280 to 777 kWh/t O_2 for ASU [21] and 265 to 460 kWh/t O_2 for PSA [22–24].

In their study, Banaszkiewicz et al. [25] compared different oxygen production technologies for Oxyfuel combustion, including ASU, PSA, and polymer and ion transfer membranes. They concluded that for large oxy-combustion power plants, the cryogenic process is the best method due to its production capacity and energy efficiency. However, the PSA technology is suitable for small-scale Oxyfuel applications and steel mills. Sulc and Ditl [21] evaluated two different oxygen sources for a small oxy-combustion unit: Pressure swing adsorption and liquid oxygen delivery. They found that the cost and CO_2 emissions of oxygen supplied by the PSA unit depend mainly on the electricity price and the emission factor for electric energy. In their case study, they show that for the operation in Germany, the on-site production via PSA leads to higher costs and CO_2 emissions compared to the delivery of oxygen produced by a large cryogenic air separation plant.

1.2.3. Power to Gas

PtG technology refers to the process of gaseous fuel production from electric energy by electrolysis (hydrogen) and optional subsequent methanation (SNG). The resulting coupling of the electricity and gas grids and the storability of the generated energy carriers represents a flexibility option [26]. Key considerations for power to gas applications are the underlying electrolysis and methanation technologies.

Electrolysis

Due to its versatile application and the omission of direct CO_2 emissions, hydrogen represents an important energy carrier for future climate-neutral energy systems. Hydrogen production via electrolysis using negative residual loads in the electricity system may provide flexibility for the future electrical grid and thus contribute to the integration of fluctuating RES.

Three main technologies are available for electrolysis, which are characterized by their respective electrolyte: Alkaline water electrolysis (AEC), proton exchange membrane electrolysis (PEM-EC), and solid oxide electrolysis (SOEC). Alkaline electrolyzers consist of an aqueous potassium hydroxide electrolyte and two nickel, cobalt, or iron electrodes separated by an insulating diaphragm [27]. They operate at temperatures of 40–90 °C, pressures from atmospheric pressure to 30 bar, and production rates of 0.01–45 kg H_2/h. Specific energy consumption lies in the range of 46–60 kWh/kg H_2. A disadvantage of the AEC is its lower partial load limit of 20–40% [28]. In PEM electrolysis cells, a proton-conducting polymer membrane substitutes the liquid electrolyte and the diaphragm and the electrodes consist of platinum group metals. At operating temperatures of 20–100 °C, pressures of 10 to 85 bar, and hydrogen production rates of 0.02–4.50 kg/h, the energy consumption rate ranges from 53–81 kWh/kg H_2 [28]. The utilization of noble metals as electrode materials leads to higher capital costs for the PEM-EC. However, an expert elicitation concludes that in the future, the PEM-EC will be favored for the integration of renewables due to significant cost reductions and its higher operational flexibility [29].

Since all the considered electrolysis technologies produce oxygen as a by-product, Kato et al. [18] propose the simultaneous utilization of hydrogen and oxygen from water electrolysis. They argue that oxygen production via electrolysis is not competitive compared to the conventional technologies. However, the utilization of by-product oxygen reduces the cost for hydrogen production and the demand for oxygen produced using air separation technologies. An economic case study investigating the operation of a PEM-EC indicates that revenues from by-product oxygen significantly reduce the hydrogen production costs.

In their study, Iora and Chiesa [30] propose the combination of a solid oxide fuel cell (SOFC) with a solid oxide electrolysis cell (SOEC) for oxygen production. The process layout aims to provide part of the electric power for the electrolysis by feeding the SOFC

with the generated hydrogen. According to a finite difference model of the SOFC/SOEC stack, the system operates at a specific energy consumption of 350–500 kWh/t O_2 under optimized conditions [31].

Methanation

In order to supply existing infrastructure with renewable gases, the hydrogen can be converted to synthetic natural gas (SNG) by methanation with carbon dioxide [27]. Methanation is a catalytic, exothermic process that converts carbon dioxide and hydrogen to methane at elevated temperature and pressure following the Sabatier reaction. The conversion process is favored at low temperature and high pressure and has an efficiency of around 83% based on the lower heating values of hydrogen and SNG. Due to the highly exothermic conversion reactions, the cooling of the reactor is crucial. The most common systems are sequential fixed-bed reactors using nickel as catalyst [32].

In their study, Bailera et al. [26] investigated the operation of a hybrid power plant combining a power-to-gas plant and an Oxyfuel combustion plant. The proposed PtG-plant consists of an alkaline electrolyzer with an efficiency of 68.1% based on LHV and a three-stage adiabatic methanation process operating at a pressure of 30 bar. By-product oxygen from the electrolysis is used in an oxy-combustion combined cycle power plant. The thereby generated carbon dioxide is recovered from the flue gas as a feedstock for the methanation process. This configuration allows for the storage of energy in the form of hydrogen or SNG and the substitution of oxygen produced by air separation. The results of a heat integration scenario investigating the exploitation of waste heat from the methanation process in the combined cycle power plant indicate an overall system efficiency of 67.8%. The authors conclude that the concept is particularly feasible for application in industrial energy systems. Similar research outlines combining catalytic methanisation and hydrogen production by electrolysis were also covered by the studies of Herrmann et al. [33], Chwola et al. [34], and Gorre et al. [17,35].

1.3. Research Need and Outline of the Article

The relevant literature covers extensive articles on commercially available and future technologies for oxygen, hydrogen, and SNG production; viable configurations for general power-to-gas plants; and technological concepts and business models for their profitable flexible operation (see Section 1.2). However, the optimal integration of such plants into an industrial production process has not yet been investigated. Therefore, we aim to identify the optimal implementation concept for the discussed technologies and evaluate their impact on the overall energy consumption, carbon dioxide intensity, and economic efficiency of the steel production process.

Therefore, we focus on the following research questions:

Q 1. *What are cost-optimal plant designs and operation modes for flexible O_2, H_2, or SNG production plants in an EAF steel mill?*

   a. Which basic plant layouts seem to be possible based on state-of-the-art technologies?
   b. Which basic operational strategies are useful under which boundary conditions?

Q 2. *What is their impact in terms of carbon dioxide emissions? How do they influence the overall energy systems with regard to their demand-side management potential (qualitatively and quantitatively)?*

Q 3. *Which economic framework conditions are required for their economically viable operation?*

In order to address these questions, we develop feasible scenarios for EAF steel mill on-site oxygen, hydrogen, and SNG production via pressure swing adsorption, electrolysis, and methanation (Section 2.1). Then, we first present an optimization model that is suited for the integration of these technologies into an existing EAF steel mill (Section 2.2); second, the deployed load profiles (Section 2.3); and third, the framework for the economical assessment (Section 2.4) are presented. Finally, we compare the scenarios based on adequate

key performance indicators (KPIs) and discuss the results from a technical and economic point of view (Section 3).

2. Materials and Methods

The following section covers the development of feasible scenarios and the setup of the optimization model.

2.1. Considered Scenarios

In order to evaluate the feasible process layout designs, we investigate the following scenarios (see Table 1):

1. The scenario PSA involves the on-site production of oxygen by a pressure swing adsorption unit. Electricity and natural gas are drawn from the grid at wholesale prices. The consumption of natural gas results in additional costs for the purchase of the related emission certificates. The implementation of the PSA into the steel mill enables the omission of oxygen purchase; however, there are additional capital costs for the installation and costs for covering the electricity demand of the oxygen production plant. The resulting levelized cost of oxygen (LCOO) serves as a benchmark for evaluating the alternative system layouts.

2. In scenario PEM, the required oxygen for the steel production process is generated as a by-product in a PEM electrolysis plant. Thus, the purchase of oxygen is obsolete in this case as well. Revenues from the sales of hydrogen aim to offset the increased expenses for investment and energy. If economically viable, a part of natural gas purchased from the grid is substituted by the produced hydrogen. Thus, we assume that the installed burners allow for the combustion of mixtures of natural gas and hydrogen up to 100% H_2. In this case, the internal hydrogen utilization saves energy costs and direct carbon dioxide emissions.

3. In scenario SNG, a share of the hydrogen from the electrolysis unit is withdrawn in order to methanize the CO_2 produced from a mill-internal carbon capture (CCU) plant. This not only ensures sufficient oxygen supply but also reduces the amount of natural gas obtained from the grid and creates a sink for carbon dioxide. However, the limited availability of captured CO_2 results in a surplus of hydrogen. In this scenario, we restrict the admixture of hydrogen into the natural gas infrastructure in the EAF steel mill to $20\%_{vol}$ of the current natural gas load. Analogous to the scenario PEM, excess hydrogen is injected into the gas grid and, therefore, represents a source of revenue.

Table 1. Summary of the investigated scenarios.

Feature	PSA	PEM	SNG
Oxygen supply	VPSA	PEM electrolysis	PEM electrolysis
Oxygen purchase	no	No	no
Hydrogen sales	no	Yes	yes
Methanation	no	No	yes
Max. Hydrogen admixture [1]	-	100%	20%

[1] For each time step, the hydrogen content of the gas that is consumed in the steel mill is limited between 0–$100\%_{vol}$ (PEM) and 0–$20\%_{vol}$ (SNG).

2.2. Optimization Model

For the optimized integration of the mentioned technologies in the existing plant, we use the open-source modeling framework *oemof* (open energy modeling framework), which serves as a multi-purpose toolbox for the modeling and optimization of energy systems. The graph-based modeling framework is realized using object-oriented programming in the language Python [36]. Due to its ability to represent multi-sectoral energy systems at various scales, its transparent continuous development process, and its extensive documentation, *oemof* is suitable for a broad range of applications [37].

Within this framework, the *oemof solph* library represents a model generator for mixed-integer linear optimization problems [38]. More precisely, *solph* provides classes with associated objective expression terms, optimization variables, and constraints. These classes are used to recreate and connect components of an actual energy system. Based on their features, the components are categorized as transformers (meaning energy conversion units), sources, and sinks. Energy systems are created by interconnecting the individual components by buses. The objective of the optimization is to minimize the total energy cost (C_{tot}) of the steel mill, which is defined in Section 2.4, within the considered time frame [37] (Equation (1)):

$$\min f = C_{tot} \tag{1}$$

$$P_{O2}(t) - D_{O2}(t) + S_{O2}(t) = 0 \tag{2}$$

$$P_{CO2} - x_{CO2} \cdot P_{SNG} = 0 \tag{3}$$

$$SR_{H2}(t) \leq SR_{H2,max} \tag{4}$$

As a constraint, we predefined that the oxygen demand of the steel mill ($D_{O2}(t)$) has to be satisfied in each time step either through production ($P_{O2}(t)$) or through the storage ($S_{O2}(t)$) without venting excess production for all scenarios (2). In the SNG scenario, all the available carbon dioxide must be used for methanation (3). P_{CO2} represents the produced amount of carbon dioxide in kg/a, x_{CO2} the specific carbon dioxide consumption for the production of one MWh of SNG, and P_{SNG} the produced amount of SNG in MWh/a. Another constraint is the compliance of the hydrogen substitution ratio ($SR_{H2}(t)$) with the limits for hydrogen admixture into the gas system ($SR_{H2,max}$) (4). The gas storages and buses are assumed to be loss-free, and the transformers are implemented with constant efficiencies. A linear model was used for the long-term optimization runs due to the insignificant error and the reduced computation time. The predefined input parameters are listed in Table 2. The load range specifies the operation window of individual units by defining the lower and upper limit as a percentage of full load based on the oxygen, hydrogen, and SNG output. The load gradient indicates the maximum load change rate as a percentage of the full load per minute.

Table 2. Parametrization of the model components.

Parameter	Unit	2020	2030	2050	Reference
VPSA unit					
Specific energy demand	kWh_{el}/kg	0.35	0.35	0.35	[22–24]
Load range	%	60–100	60–100	60–100	own assumption
Load gradient	%/min	4	4	4	own assumption
Pressure	Mpa	3	3	3	[28]
PEM electrolysis unit					
Efficiency	kWh_{H2}/kWh_{el} [1]	0.68	0.75	0.83	[39–41]
Specific energy demand H_2	kWh_{el}/kg	58.0	52.6	47.5	own calculation
Specific energy demand O_2	kWh_{el}/kg	7.3	6.6	6.0	own calculation
Load range	%	0–100	0–100	0–100	[35]
Methanation unit					
Efficiency	kWh_{SNG}/kWh_{H2} [1]	0.62	0.62	0.62	own calculation, [42]
Load range	%	20–100	20–100	20–100	[33]
Load gradient	%/min	3	3	3	[35]
Buffer storage					
Minimum pressure	MPa	1	1	1	own assumption, [35]
Maximum pressure	Mpa	3	3	3	own assumption, [35]
O_2 compressor					
Mean pressure	Mpa	2	2	2	own assumption
Specific energy demand	kWh_{el}/kg_{O2}	0.14	0.14	0.14	own calculation
H_2 compressor					

Table 2. *Cont.*

Parameter	Unit	2020	2030	2050	Reference
Mean pressure	Mpa	35	35	35	own assumption
Specific energy demand CO_2 compressor	kWh_{el}/kg_{H2}	2.14	2.14	2.14	own calculation
Mean pressure	Mpa	2	2	2	own assumption
Specific energy demand	kWh_{el}/kg_{CO2}	0.09	0.09	0.09	own calculation

[1] based on HHV.

The purchase of electricity, natural gas, and CO_2 emission allowances and the installation of production and storage capacities are associated with costs, whereas the sales of hydrogen and SNG generate revenues. The adopted specific CAPEX (capital expenditures) and OPEX (operational expenditures) and the commodity prices are listed in Tables 3 and 4. Each optimization run covers one year with a resolution of 30 min for each time-step. In order to obtain the minimum costs under these conditions, it is necessary to optimize both the sizing of the equipment and its operation.

Figure 1 gives an overview of the optimization model, which consists of buses, transformers, storages, sinks, and sources. The model covers the commodities electricity, hydrogen, natural gas, SNG, oxygen, and carbon dioxide, which are represented by energy buses. The production plants for water and oxygen and the methanation unit are implemented into the model as transformers. Furthermore, every commodity bus is connected to a storage and to either external sources (purchase) or sinks (sales).

2.3. Load Profiles

The load profiles for electricity demand and for the demand for natural gas and oxygen consumed in the steel mill are obtained from an energy system model developed and extended by the authors in previous studies [6,9]. This model describes a steel mill that produces heat-treated high-alloyed steel ingots from 100% steel scrap using a 65 t alternating current (AC) EAF. Figure 2 gives a rough overview of the production process and the most important energy consumers.

While the electricity demand results mainly from the EAF operation, the natural gas demand is due to the following consumers:

- Ladle heaters;
- Annealing furnaces;
- Other consumers.

The oxygen demand profile results from the oxygen demands at the following consumers:

- Electric arc furnace;
- Vacuum oxygen decarburization units;
- Ladle heaters;
- Other consumers.

Considering the operation of the electric arc furnace, oxygen demand occurs during two process phases that require different oxygen flow levels: low mass flow rate for the melting phase and high mass flow during refining. The oxygen demand for the VOD process is to be constant during the VOD treatment time while the demand of the Oxyfuel ladle heaters is proportional to their natural gas consumption and is defined by the oxidant/fuel ratio. For the mill size-independent system analysis, we use normalized load profiles. Therefore, we relate the demand in each time step to the peak demand. Figure 3 shows the normalized demand profiles of electric power, natural gas, and oxygen for one week generated by the energy system model of the EAF steel mill.
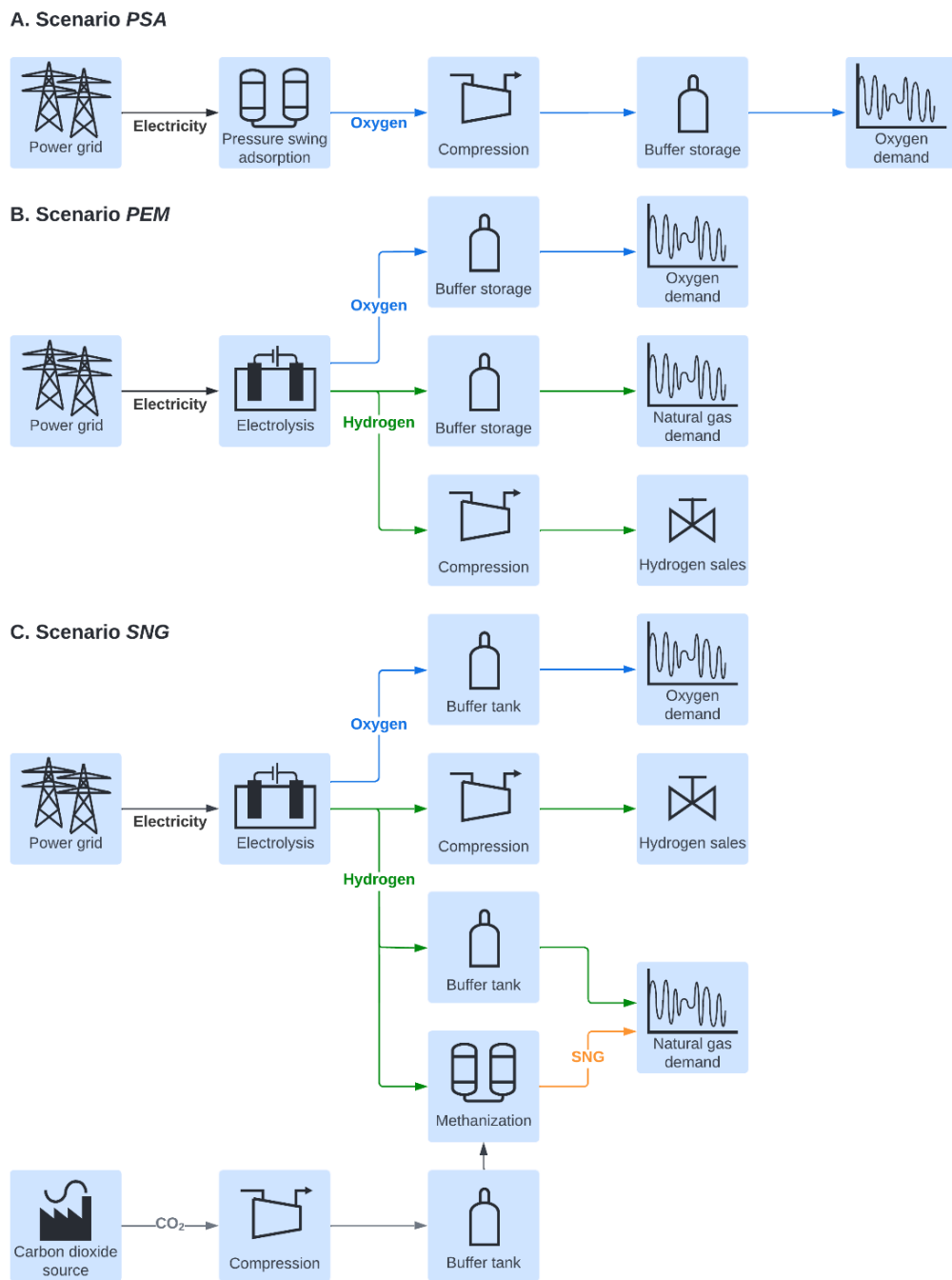
A. Scenario *PSA*

B. Scenario *PEM*

C. Scenario *SNG*

Figure 1. Configuration of the optimization model for the individual scenarios.
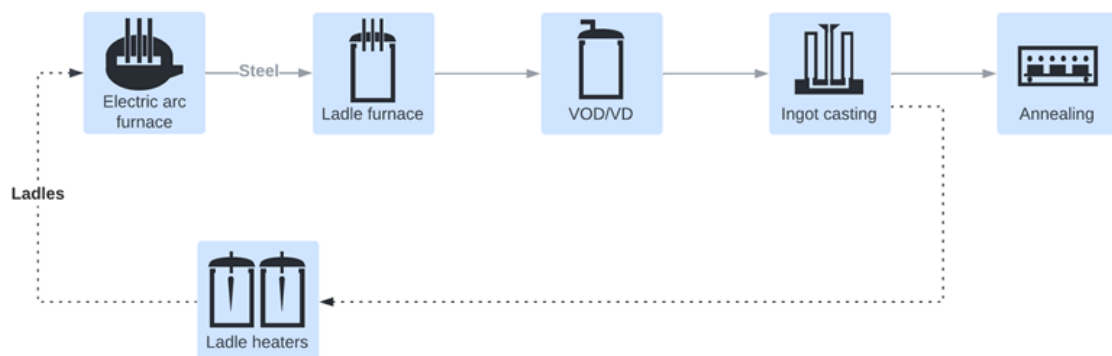
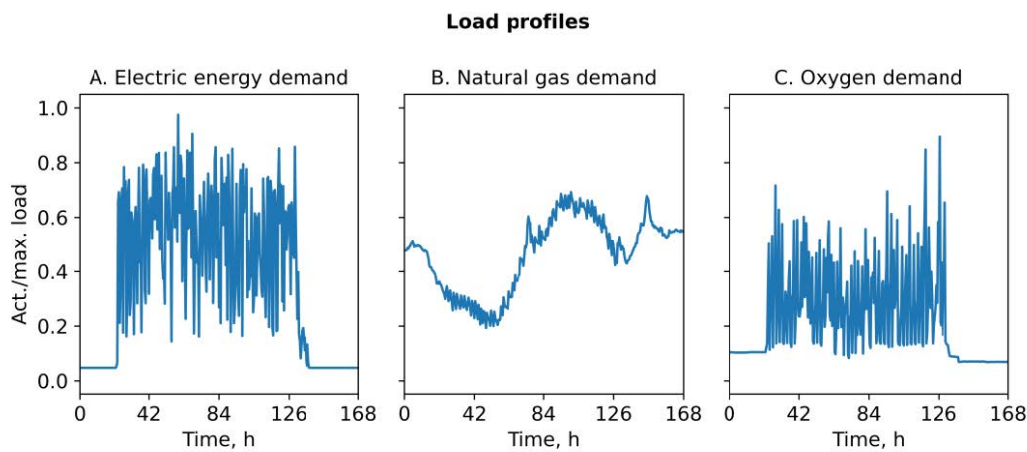**Figure 2.** Production process scheme of the considered EAF steel mill.

Figure 3. Demand profiles for electric power (**A**), natural gas (**B**), and oxygen (**C**).

2.4. Cost Model

The optimization aims at minimizing the total energy costs (C_{tot}) of the steel mill in MEUR within the considered period of a year. Therefore, the cost model includes annual capital (A_{CAPEX}) and annual operational expenditures (C_{OPEX}) for production, compression, and storage of the product gases and the energy costs (C_{energy}, Equation (10)) for the overall steel mill reduced by the revenues from hydrogen sales ($R_{H2\ sales}$) (see Equation (5)):

$$C_{tot} = A_{CAPEX} + C_{OPEX} + C_{energy} - R_{H2\ sales} \tag{5}$$

Additionally, the economic performance of the hydrogen scenarios (PEM and SNG) is compared based on the levelized cost of hydrogen (LCOH) and levelized cost of methane (LCOM) in EUR/MWh$_{HHV}$ (c_{H2} and c_{SNG}). The LCOH is obtained from Equation (6), where $A_{CAPEX,\ H2}$, $A_{CAPEX,\ O2}$, $C_{OPEX,\ H2}$, and $C_{OPEX,\ O2}$ are the annual capital and operational expenditures for the oxygen and hydrogen supply equipment. c_{O2} represents the LCOO in the PSA scenario (see Equation (8)) and P_{H2} and P_{O2} are the annual hydrogen and oxygen production in MWh/a and t/a, respectively. The LCOM is determined using Equation (7), where $A_{CAPEX,\ SNG}$, $A_{OPEX,\ SNG}$, and $C_{energy,\ SNG}$ are the annual capital, operational, and energy costs for SNG production. M_{H2} is the amount of hydrogen supplied to the methanation plant and P_{SNG} is the annual SNG production:

$$c_{H2} = \frac{A_{CAPEX,\ H2} + A_{CAPEX,\ O2} + C_{OPEX,\ H2} + C_{OPEX,\ O2} + C_{energy,\ H2} - c_{O2} \cdot P_{O2}}{P_{H2}} \tag{6}$$

$$c_{SNG} = \frac{A_{CAPEX,\ SNG} + A_{OPEX,\ SNG} + C_{energy,\ SNG} + c_{H2} \cdot M_{H2}}{P_{SNG}} \tag{7}$$

$$c_{O2} = \frac{A_{CAPEX,\ O2} + C_{OPEX,\ O2} + C_{energy,\ O2}}{P_{O2}} \tag{8}$$

Most of the studies cited in this article anticipate that both energy and capital costs for power-to-gas technologies will change substantially over the period between 2020 and 2030. The volatility of energy costs is underlined by the 2022 distortions on global energy markets, caused by the Russian attack on Ukraine. In order to analyze the impact of variable commodity prices and investment costs, we assess all scenarios based on the historical costs of 2020 and on projected costs for the years 2030 and 2050. All projections are based on high-level studies for the European energy markets [43,44].

2.4.1. Equipment Cost

Table 3 provides a breakdown of the costs and lifetimes of individual plant components. In 2013, with specific investment costs of around 2000 EUR/kW, PEM electrolysis plants were about twice as expensive as their alkaline counterparts [28], whereas more recent data

from 2018 cites costs from 1000 to 1500 EUR/kW for both alkaline and PEM systems [45]. A report commissioned by the Fuel Cells and Hydrogen Joint Undertaking estimates that the system costs for PEM electrolysis will decrease from 700–1300 EUR/kW in 2020 to 250–1270 EUR/kW by the year 2030 [46]. For the methanation unit, specific investment costs of 450 EUR/kW of synthetic natural gas are estimated [35]. For the calculation of the annual capital costs for the implemented equipment, we assume an interest rate of 4% [8]. Typical operational costs for the implemented equipment are fixed at 1 to 3% of CAPEX per year [35,46].

Table 3. Specific equipment costs for the years 2020, 2030, and 2050.

Cost Component	Unit	2020	2030	2050	Reference
VPSA unit					
CAPEX	EUR/kW$_{el}$	3000	3000	3000	calculated from [21]
OPEX	%$_{CAPEX}$	2	2	2	own assumption
Lifetime	a	10	10	10	[21]
PEM electrolysis unit					
CAPEX	EUR/kW$_{el}$	1000	750	500	[39,46]
OPEX	%$_{CAPEX}$	2.75	2.75	2.75	[35]
Lifetime	a	20	20	20	[35]
Methanation unit					
CAPEX	EUR/kW$_{SNG}$	450	450	450	[35]
OPEX	%$_{CAPEX}$	3	3	3	[35]
Lifetime	a	20	20	20	[35]
Buffer storage					
CAPEX	EUR/m^3	50	50	50	[35,45]
OPEX	%$_{CAPEX}$	1	1	1	[35]
Lifetime	a	20	20	20	[35]
O$_2$ compressor					
CAPEX	EUR/kW$_{el}$	1100	1100	1100	calculated from [47]
Lifetime	a	10	10	10	own assumption
H$_2$ compressor					
CAPEX	EUR/kW$_{el}$	700	700	700	calculated from [47]
Lifetime	a	10	10	10	own assumption
CO$_2$ compressor					
CAPEX	EUR/kW$_{el}$	1480	1480	1480	calculated from [47]
Lifetime	a	10	10	10	own assumption

Investment costs for the PSA, electrolysis, and methanation plants and the storage tanks and compressors are allocated to the assessment period by applying the annuity method (9). The annuity (A_{CAPEX}) is calculated by multiplying the investment costs for the individual assets (I) by an annuity factor, which depends on the interest rate (i) and the depreciation period (n). The individual assets are depreciated over their useful life to facilititate the economic comparison of different technologies using levelized costs:

$$A_{CAPEX} = I \cdot \frac{(1+i)^n \cdot i}{(1+i)^n - 1} \tag{9}$$

2.4.2. Energy Costs

In terms of energy costs, we take into account the purchase of electrical energy, natural gas, and carbon dioxide emission allowances (see Equation (10)). p_{EE}, p_{NG}, and p_{EA} represent the prices for electric energy, natural gas, and emission allowances in EUR/kWh and EUR/t$_{CO2}$, respectively; D_{EE} and D_{NG} are the respective demand both in kWh/h, and SR is the substitution rate of natural gas either by hydrogen or SNG in %$_{HHV}$. SCE represents the specific carbon dioxide emissions of natural gas in kg/kWh$_{CH4}$:

$$C_{energy} = \sum_t D_{EE}(t) \cdot p_{EE}(t) + D_{NG}(t) \cdot (1 - SR(t)) \cdot (p_{NG} + SCE \cdot p_{EA}) \tag{10}$$

In our model, surplus hydrogen in kg/h ($M_{H2\ surplus}$) is sold at a fixed price in EUR/kg$_{H2}$ (p_{H2}), generating annual revenues in EUR/a ($R_{H2\ sales}$) that contribute to covering the total costs (11):

$$R_{H2\ sales} = \sum_t M_{H2\ surplus}(t) \cdot p_{H2} \tag{11}$$

For the 2020 scenario, we adopt the historical 2020 spot market prices, whereas for the future scenarios, estimated prices for the year 2030 are applied. In 2020, the average day-ahead electricity price at the Energy Exchange Austria (EXAA) was 33 EUR/MWh with a standard deviation of 17 EUR/MWh [48]. The development of electricity prices between 2020 and 2050 reflects the higher demand of flexibility options to balance demand and production, the rising primary energy demand, and the anticipated price surge for CO_2 emission allowances [43]. To cope with the mentioned influence factors on electricity prices, two aspects are considered for the estimated electricity price forecasts for 2030 and 2050:

- The development of the annual mean value of the electricity price [44]; and
- The development of the number of extreme price situations (higher than 100 €/MWh and lower than 0 €/MWh) [43].

However, the current (2022) situation on the energy markets makes it necessary to mention the high degree of uncertainty of such price projections. In the approach proposed by Taupmann et al. [49], first, the historical quarter-hourly spot market price profile from 2020 is scaled based on the predicted annual mean prices in 2030 and 2050 obtained from the EU Energy Outlook [44]. However, extreme price situations are not sufficiently represented by this scaling. To depict them, the duration curves of the scaled price profiles are additionally fitted. The resulting duration curves not only reflect the annual mean values but also the number and duration of extreme price situations estimated in the literature [43,44]. Finally, the individual quarter-hourly electricity prices in the annual profile are adjusted according to the fitted duration curve. This approach results in a mean electricity price of 62 EUR/MWh with a standard deviation of 37 EUR/MWh for 2030 and a mean electricity price of 82 EUR/MWh with a standard deviation of 66 EUR/MWh for 2050. Figure 4 compares the day-ahead prices traded at the EXAA in 2020 with those predicted for 2030 and 2050. Both the price profile (A) and the ordered duration curve (B) reflect the rising average and the increasing extreme prices through 2050.
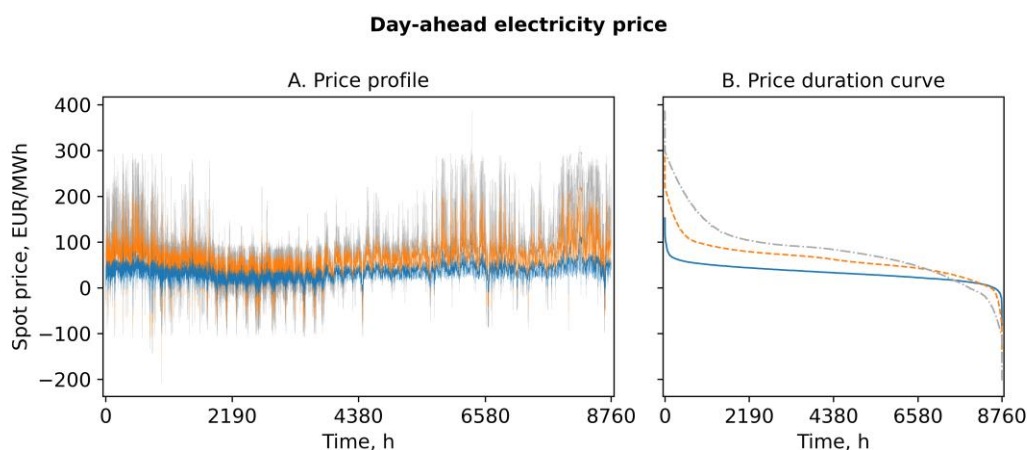

Figure 4. Comparison of the historical and forecasted (FC) electricity wholesale price profiles (**A**) and duration curves (**B**) for 2020 (blue), 2030 (orange), and 2050 (grey).

In its World Energy Outlook 2021, the IEA [50] provides forecasts on natural gas prices in the European Union. Starting from 13 EUR/MWh in 2020, the net-zero emissions scenario projects a slight decrease in wholesale prices to 12 EUR/MWh in 2030 and 11 EUR/MWh in 2050. Additionally, here, it needs to be said that the actual unclearness on the natural gas market leads to a lack of meaningful price prognoses. The prices used for

this work are based on data published before the Ukrainian war and should, therefore, be treated as data with high uncertainty.

The mean prices for emission allowances are assumed to increase from 24 EUR/t CO_2 in 2020 [51] to 130 EUR/t CO_2 in 2030 [50,52] and 250 EUR/t CO_2 in 2050 [50]. In their study on the integration of hydrogen into the natural gas system, Cvetkovska et al. [53] expect the cost of hydrogen to fall from 146 EUR/MWh in 2020 to 61 EUR/MWh in 2050. Table 4 summarizes the estimated wholesale prices for different energy carriers, gases, and emission allowances.

Table 4. Commodity wholesale prices for the years 2020, 2030, and 2050.

Cost Component	Unit	2020	2030	2050	Reference
electric energy (mean)	EUR/MWh	33	62	82	[43,44,48]
natural gas	EUR/MWh$_{HHV}$	13	12	11	[50]
hydrogen	EUR/MWh$_{HHV}$	146	101	61	[53]
emission allowances	EUR/t	24	130	250	[50–52]

The listed prices for natural gas are surcharged by grid charges of 2.2 EUR/MWh [54], a natural gas levy of 5.8 EUR/MWh, and a value added tax of 20% [55]. Regarding the electricity prices, these differ between PSA and electrolysis units: For the PSA unit, the electricity costs include grid charges of 18 EUR/MWh [56], an electricity levy of 15 EUR/MWh, and a value added tax of 20% [57], whereas for the electrolysis unit (scenario *PEM* and *SNG*), only the wholesale power price is considered. This approach is based on the assumption that production plants for green gases are not subject to grid charges [58]. Moreover, we stipulate that due to their system-serving operation, all the gas production facilities are exempt from other fees and taxes on electric energy.

3. Results and Discussion

In the following section, we will present the results of our optimization-based investigations. According to our research questions (see Section 1.3), we will analyze the scenarios, with a focus on demand-side management and carbon dioxide emissions. We will formulate feasible strategies for an economically viable operation of the explained technologies to be integrated.

3.1. General Results

Figure 5 describes the supply of the time-resolved oxygen demand by the PSA unit for one week in the years 2020, 2030, and 2050. Owing to its limited load range, the PSA unit is continuously in operation, with the demand peaks that occur between hour 30 and 130 being covered by the storage tank. In addition, the high share of CAPEX in the LCOO and the lack of opportunities for product sales obliges the plant to operate at high full-load hours, regardless of the electricity prices. This is substantiated by the fact that the plant operates at full load during periods of low demand and on weekends. Hence, the mode of operation does not change throughout the years 2020 to 2050.

In contrast, the electrolysis implemented in scenario PEM operates over the full load range, depending on the hydrogen and oxygen demand and electricity prices. As indicated by Figure 6, it shuts down during periods of high electricity prices, meets the oxygen demand from the storage, and refills it during periods of lower prices. Therefore, the increase in electricity price volatility from 2020 to 2050 results in more frequent and longer periods of production interruptions and an extensive exploitation of the available load range.
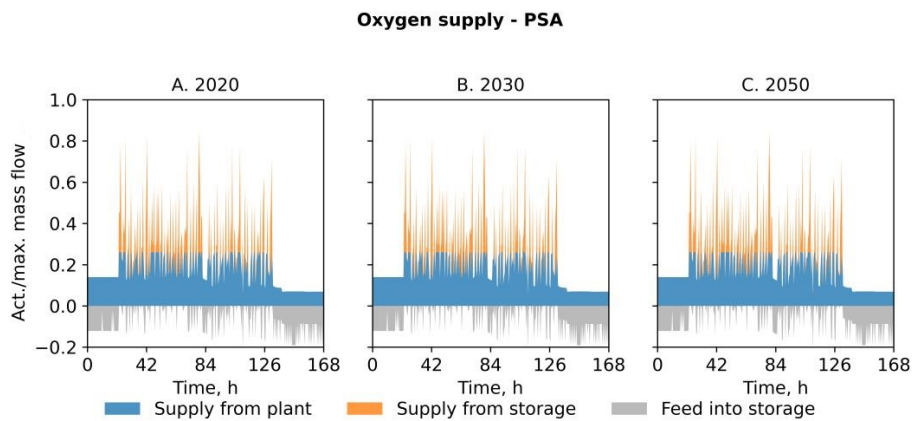
Oxygen supply - PSA

Figure 5. Covering the oxygen demand of the steel mill deploying a PSA for oxygen production in the years 2020 (**A**), 2030 (**B**) and 2050 (**C**).
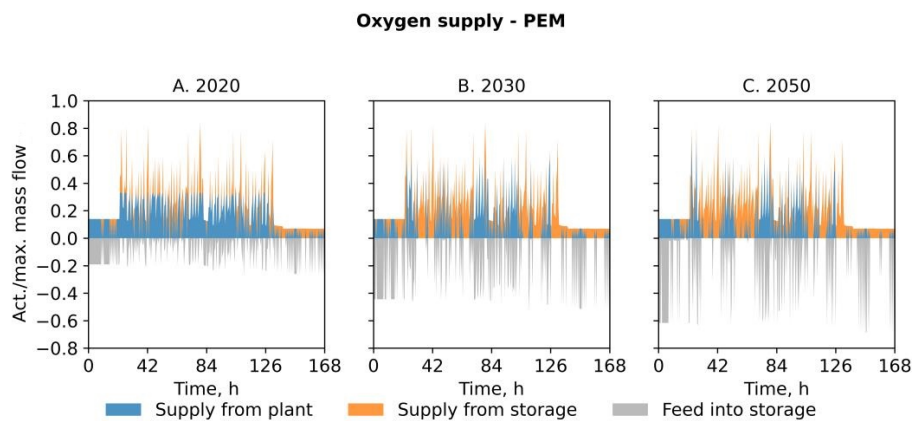
Oxygen supply - PEM

Figure 6. Covering the oxygen demand of the steel mill deploying PEM electrolysis for hydrogen and oxygen production in the years 2020 (**A**), 2030 (**B**) and 2050 (**C**).

The oxygen supply profile in the scenario SNG, which is depicted in Figure 7, features individual production peaks that increase with a growing number of extreme price situations and a decreasing specific CAPEX towards 2050. The constant operation of the electrolysis unit, which is particularly visible in the year 2050, is caused by the limited operating window of the methanation unit and the boundary condition that all CO2 must be used for methanation. Apart from that, this configuration provides a comparable degree of flexibility as the PEM scenario.
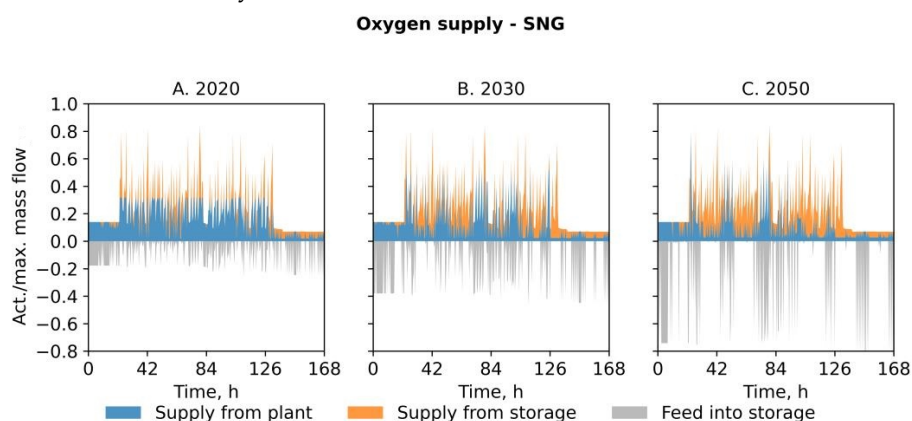
Oxygen supply - SNG

Figure 7. Covering the oxygen demand of the steel mill deploying PEM electrolysis for oxygen and hydrogen and a subsequent methanation unit for SNG production in the years 2020 (**A**), 2030 (**B**) and 2050 (**C**).

Table 5 lists the indicators derived from the time series that were obtained from the optimization model. The nominal power of the electrolysis system (scenario PEM and SNG) clearly exceeds that of the PSA unit in all scenarios. On the one hand, the specific energy demand for electrolysis is about ten times higher than for pressure swing adsorption. On the other hand, the latter produces the same amount of oxygen at less full-load hours. The annual net production of 42 GWh of hydrogen in scenarios PEM and SNG offsets the higher energy consumption of the PEM unit. Since the production units have to meet the specified oxygen demand profile without venting excess oxygen, the production volumes of oxygen, hydrogen, and SNG in the PEM and SNG scenarios remain constant over the investigated years.

Table 5. Resulting key performance indicators for the optimization scenarios.

KPI	Unit	2020			2030			2050		
Scenario	-	PSA	PEM	SNG	PSA	PEM	SNG	PSA	PEM	SNG
Nominal power	kW_{el}	400	10,600	10,185	400	16,900	15,100	400	20,000	23,300
Full-load hours	hrs	7439	5876	6119	7439	3325	3738	7439	2567	2202
H2 production	MWh_{HHV}/a	-	42,400	42,400	-	42,400	42,400	-	42,400	42,400
SNG production	MWh_{HHV}/a	-	-	8600	-	-	8600	-	-	8600
CAPEX share	%	45	30	30	37	31	28	34	32	36
Fuel substitution	$\%_{HHV}$	-	0	15	-	0	15	-	45	19

The electrolysis operation depends not only on the electricity price and oxygen demand but also on the natural gas demand. The fuel substitution is a measure for the internal utilization of the produced hydrogen and SNG in the steel mill. In the years 2020 and 2030, it is more profitable to sell the hydrogen and procure natural gas from the grid. In the absence of economic alternatives, merely the produced SNG is consumed as a fuel. Conversely, in the PEM 2050 scenario, 45% of the gas demand is covered by on-site produced hydrogen. In scenario SNG, the restriction of the limited admixture of natural gas into the internal gas network implies that the major share of hydrogen must be sold, even if the on-site substitution of natural gas was more cost efficient. However, this leads to higher flexibility and thus the improved exploitation of favorable electricity prices. As a result, the SNG 2050 scenario achieves lower full-load hours than the PEM 2050 scenario.

3.2. Demand-Side Management Potential

A comparison of both the supply profiles (Figures 5–7) and the full-load hours (Table 5) indicates that the electrolysis-based scenarios (PEM, SNG) provide more flexibility with respect to a power price-driven operation schedule compared to the *PSA* scenario. However, the number of full-load hours alone is not a sufficient indicator for evaluating the plant concepts regarding the demand-side management potential. For CAPEX-intensive plants (scenario PSA), the optimizer tends to meet the specified oxygen demand with the minimum installed production and storage capacity, without considering the electricity price. In this case, the oxygen load profile determines the full-load hours rather than the electricity price signal.

Therefore, the mean price of purchased electrical energy, referred to as the effective average price ($p_{effective\ average}$), for the individual gas production units was considered to assess the flexibility potential of the different scenarios (see Table 6). $p_{effective\ average}$ is determined according to Equation (12), where $p_{EE}(n)$ represents the electricity price and $D_{EE}(n)$ is the demand for electric energy for each time step n:

$$p_{effective\ average} = \frac{\sum_{n=1}^{t} p_{EE}(n) \cdot D_{EE}(n)}{\sum_{n=1}^{t} D_{EE}(n)} \tag{12}$$

Table 6. Annual, ordered, and effective electricity prices for 2020, 2030, and 2050.

Electricity Prices	Scenario	Unit	2020	2030	2050
Annual average	-	EUR/MWh	33	62	82
Ordered average	PSA	EUR/MWh	28	51	62
	PEM	EUR/MWh	24	29	11
	SNG	EUR/MWh	25	32	4
Effective average	PSA	EUR/MWh	49	76	94
	PEM	EUR/MWh	28	38	34
	SNG	EUR/MWh	28	41	33

For orientation, the effective average price and the annual average price defer in terms of the number of time steps being used for their calculation: For the calculation of the annual average price, all time steps of a year (15×8760) are taken into account. For the calculation of the effective average price, only these time steps are used in which the respective plant is actually operating. The ordered average price, however, takes into account only the cheapest electricity prices for the same number of time steps. Equation (13) specifies the relationship between the price duration curve (*DC*) and its ordered average ($p_{ordered\ average}$) at any given number of load hours (*t*):

$$p_{ordered\ average}(t) = \frac{1}{t} \cdot \sum_{n=1}^{t} DC(n) \tag{13}$$

The difference between the effective and ordered average price is a measure of how effective the respective plant is operated in terms of using low electricity prices for its operation. For the comparison of the three supply systems, the presented effective average price of the PSA was adjusted by subtracting taxes and grid charges (see Section 2.4.2).

Figure 8 depicts the ordered average price as a function of the number of full-load hours that is derived from the price duration curve. Moreover, the optimization results for the three scenarios are marked in the diagram, based on the mean purchased electricity price and full-load hours. The closer the points in Figure 8 are to the mean price curve, the more effectively the plant exploits periods of low power prices. In this context, the curve represents the border case: When the effective average prize equals the ordered average for the considered number of full-load hours, the plant provides the maximum flexibility. The data in Tables 5 and 6 supports the previously observed findings: The electrolysis-based scenarios feature the highest degree of flexibility. This is reflected by significantly less full-load hours and a lower effective average price compared to the PSA unit throughout the years 2020, 2030, and 2050.

3.3. Carbon Dioxide Emissions

For the calculation of carbon dioxide emissions, we assume that the oxygen and hydrogen production plants are supplied solely with zero-emission electricity from renewable generation. Regarding the oxygen production, the CO_2 emissions attributable to scope 2, which are dependent on the specific emissions of electricity generation, are cut down to zero in the scenario PSA by this measure. Under the same assumption, scope 2 emissions are eliminated and in scenario PEM and SNG. In addition, due to the generation of CO_2-neutral energy carriers such as hydrogen and SNG, fossil fuels such as natural gas are substituted.
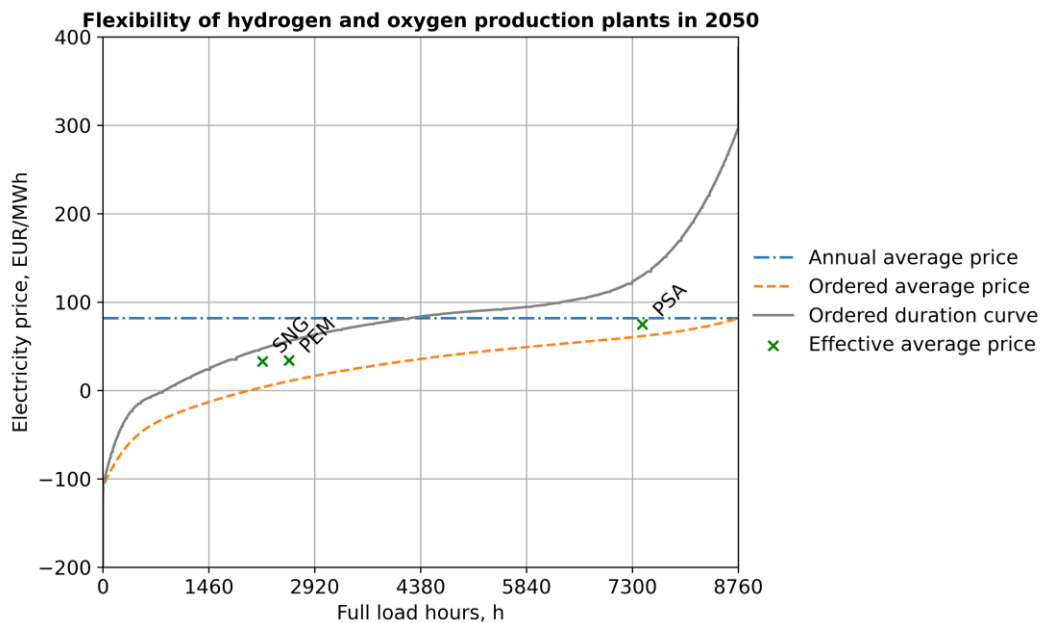
Figure 8. Purchased electricity price in relation to full-load hours.

Figure 9 shows the normalized gas demand profile that is covered by natural gas from the grid and SNG and hydrogen from on-site production for one week. In scenario PEM, the unlimited range for hydrogen admixture results in the substitution of the entire natural gas demand by hydrogen in several time steps. In scenario SNG, the specified maximum hydrogen content in the fuel and the availability of carbon dioxide for methanation are limiting the substitution of natural gas by hydrogen and SNG. Both scenarios, however, lead to substantial natural gas and carbon dioxide emission savings.
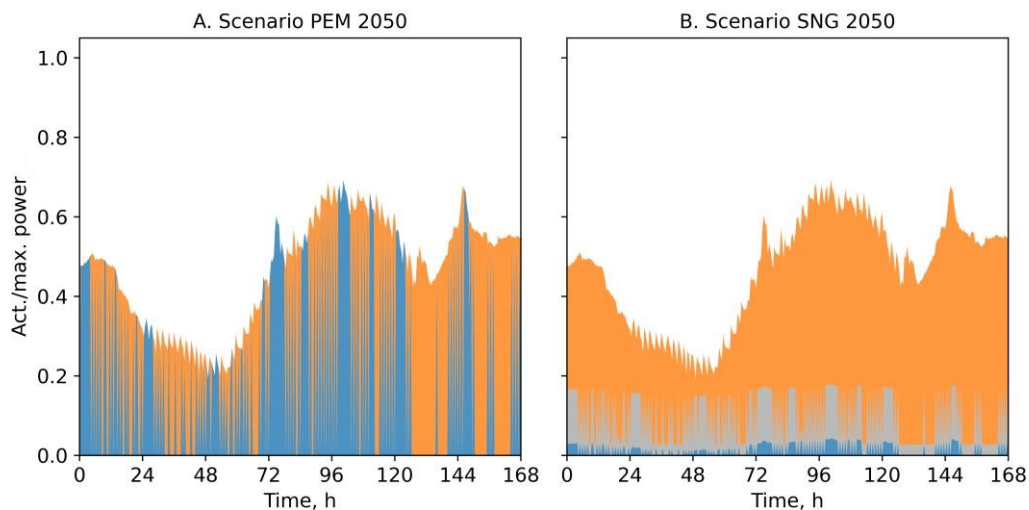
Direct fuel substitution

Figure 9. Substitution of natural gas (orange) by hydrogen (blue) and SNG (grey) for the scenarios PEM 2050 (**A**) and SNG 2050 (**B**).

Depending on where the produced gases are deployed, CO_2 emissions are reduced either within the steel mill (internal reduction) and/or in the higher-level energy system (external reduction). If hydrogen and SNG are consumed directly in the steel mill, scope 1 emissions of the steel mill are reduced. The injection of climate-neutral gases into the public gas grid reduces the specific emissions of the overall gas system. Since the amount of produced hydrogen and therefore that of substituted natural gas is constant over the

years, the total annual CO_2 emission savings amount to 7100 t for all PEM scenarios (see Table 7). In 2020 and 2030, the sale of hydrogen is more profitable than internal admixture, thus emissions are only reduced externally. In scenario PEM 2050, due to the internal utilization of hydrogen, 4600 t were saved as scope 1 emissions within the EAF steel mill and an additional 2500 t in the higher-level energy system. In the SNG scenarios, the total annual emission cut decreases to 6300 t due to the energy losses related to the methanation process. The mill-internal SNG admixture reduces internal emissions by 1500 t. Compared to scenario PEM 2050, the hydrogen admixture limit in scenario SNG 2050 constrains the steel mill-internal scope 1 emission reduction to an additional 300 t. However, the injection of excess hydrogen into the gas grid results in annual CO_2 emission savings of 4500 t CO_2 in the higher-level energy system.

Table 7. Reduction of internal (scope 1) and external (grid) CO_2 emissions.

KPI	Unit	2020		2030		2050	
Scenario	-	PEM	SNG	PEM	SNG	PEM	SNG
Internal	t_{CO2}	7100	4800	7100	4800	2500	4500
External	t_{CO2}	0	1500	0	1500	4600	1800
Total	t_{CO2}	7100	6300	7100	6300	7100	6300

3.4. Economic Assessment

In our case study, the specific costs for on-site production of oxygen via PSA will increase through 2050 due to growing electricity prices (Table 5). The scenarios involving the operation of an electrolysis plant (PEM and SNG) are also affected by increasing electricity prices. In addition, they cause substantially higher investment and energy costs. However, revenues from the hydrogen sales and savings from the substitution of natural gas by hydrogen or SNG compensate for higher costs. Consequently, the prices for electricity, natural gas, and CO_2 emission allowances are crucial for an economical operation of a power-to-gas plant. Table 6 demonstrates that the higher flexibility of the electrolysis will result in lower effective average electricity costs under highly fluctuating electricity prices in 2050 than under moderate power prices and less price volatility in 2030. In addition, specific CAPEX, especially for electrolysis units, will decrease over time.

Table 8 compares the levelized cost of hydrogen (LCOH) and SNG (LCOM) at the investigated power-to-gas plant against a reference LCOH ($LCOH_{REF}$). The LCOO is determined by the PSA scenario, which is excluded from the following analysis due to the absence of hydrogen production. As a benchmark, we take into account the levelized costs that are achieved by the electrolysis units with the capacities and full-load hours specified in Table 5 without oxygen utilization. For this purpose, we assume that the units operate under nominal load and obtain electricity at the respective ordered average price (see Table 6).

Table 8. Comparison of the levelized cost of oxygen, hydrogen, SNG, and the reference LCOH.

KPI	Unit	2020		2030		2050	
Scenario	-	PEM	SNG	PEM	SNG	PEM	SNG
LCOO	EUR/MWh_{HHV}	77	77	93	93	103	103
LCOH	EUR/MWh_{HHV}	52	52	65	66	47	50
LCOM	EUR/MWh_{HHV}	-	94	-	120	-	97
$LCOH_{REF}$	EUR/MWh_{HHV}	77	78	87	90	43	35

In the years 2020 and 2030, the LCOH in both the PEM and SNG scenario significantly undercuts the reference price due to the additional oxygen utilization. Only in 2050, the LCOH of these scenarios exceeds the reference value. In view of the given oxygen demand, the PtG plant is increasingly incapable of optimally exploiting the highly fluctuating and, above all, seasonally varying electricity price. The rising average electricity price leads to

an increasing LCOO for the relatively inflexible operation of the PSA. This also increases the cost savings from the oxygen utilization in the electrolysis scenarios. Owing to the higher CAPEX and OPEX and the energy losses, the LCOM clearly exceeds the LCOH.

Figure 10 indicates the estimated LCOH; the natural gas price, including CO2 emission allowances, charges, and taxes as described in Section 2.4.2; and the hydrogen prices for 2020, 2030, and 2050. In 2020 and 2030, the spread between the LCOH and the anticipated sales price suggests a highly profitable operation of the electrolyzer. However, in reality, there is a lack of the necessary infrastructure and the market for renewable hydrogen. The cost-efficient substitution of natural gas by internal admixture of hydrogen or injection into the gas grid is impeded by the low natural gas prices. Finally, starting at point P1, the substitution of natural gas with hydrogen is economically viable; from point P2, internal hydrogen utilization is more cost efficient than sales. Since LCOM exceeds the price of natural gas, including the emission costs, in all years, SNG production is not profitable based on the underlying conditions.
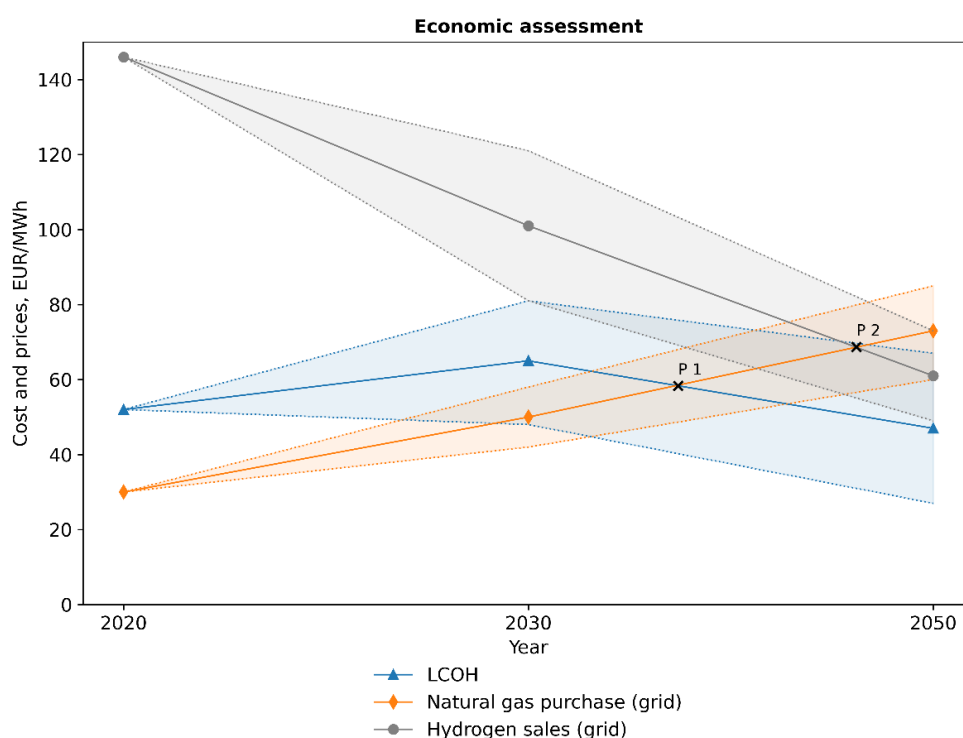

Figure 10. Comparison of the levelized cost of hydrogen and SNG with natural gas and hydrogen prices.

In view of the high degree of uncertainty regarding the assumptions for future years, we performed a sensitivity analysis: The prices for electricity on the day-ahead spot market, CO_2 emission allowances, natural gas, and hydrogen sales each varied by 20%. The dashed lines in Figure 10 represent the maximum deviations from the anticipated costs and prices from the original scenarios. According to our analysis, the substitution of natural gas by hydrogen based on PEM electrolysis while utilizing the by-product oxygen is economically viable under the condition of rising CO_2 certificate prices, highly volatile electricity prices, and declining electrolyzer CAPEX. Under the stated assumptions, this situation is likely to occur between 2030 and 2050. In contrast, due to the higher levelized cost, the replacement of natural gas with SNG is only economically viable in the event of an extreme rise in natural gas and/or CO_2 emission allowance prices (see Table 8). Therefore, the current surge of emission certificate and natural gas prices might enable investments in technologies for a climate-neutral energy supply.

4. Conclusions

In the conclusion, we present concise qualitative and quantitative answers to the research questions formulated in Section 1.3:

Q 1.a. *Which basic plant layouts seem to be possible based on state-of-the-art technologies?*

The results of the optimization suggest that all of the three investigated system layouts, including the implementation of a PSA unit, a PEM electrolysis plant, and a combination of electrolysis and methanation, are feasible options for the oxygen supply of the steel mill. If the gas infrastructure such as burners, piping, and fittings are compatible with natural gas-hydrogen mixtures, the co-production of hydrogen and oxygen by electrolysis followed by the direct utilization of both product gases is the best option in terms of energy efficiency, carbon dioxide reduction, and economic viability. From the point at which the LCOH falls below the price of natural gas, including the cost for emission allowances, the admixture of hydrogen into the gas network becomes viable. Exchanging gas with the grid eliminates the need to implement storage and allows for arbitrage operation. After subtracting the costs for oxygen supply resulting from the PSA scenario, the optimized plant configuration yields an LCOH of 47 EUR/MWh in 2050. If the implemented infrastructure is not hydrogen compatible, the methanation of CO_2 offers an alternative. The use of CO_2 from combustion processes for methanation enables the production of a carbon-neutral fuel. However, the conversion of hydrogen to methane implies higher capital and operational expenditures and energy losses, resulting in LCOM of 97 EUR/MWh in 2050. Moreover, ensuring sufficient availability of carbon dioxide is a critical prerequisite. Therefore, SNG production is not profitable under the defined framework conditions but qualifies as a bridging technology facing the limited hydrogen compatibility of the gas infrastructure.

Q 1.b. *Which basic operational strategies are useful under which boundary conditions?*

Considering the high share of electricity cost in the levelized cost of oxygen and hydrogen, it is essential to minimize the effective average electricity prices. Therefore, with increasing electricity price fluctuations and decreasing specific CAPEX for the electrolysis plant over time, larger hydrogen production capacities are advantageous, despite lower full-load hours. Adequate buffer storage capacity for produced gases is required in all scenarios not only to balance supply and demand but also to ramp up production in periods of favorable electricity prices and thus cut down on effective electricity prices.

Q 2. *What is their impact on the overall energy system in terms of demand-side management potential and carbon dioxide emissions?*

Due to the narrow load range and the high specific investment costs, the PSA offers limited demand-side flexibility. The potential CO_2 emission savings are restricted to the reduction of specific CO_2 emissions of the supplied power (scope 2). The scenarios based on electrolysis (PEM and SNG), however, show a high degree of flexibility. This is reflected by less full-load hours in the range of 3300–3700 h in 2030 and 2200–2600 h in 2050 and 46–65% lower effective average electricity prices compared to the PSA scenario. Assuming that the electrolysis process is supplied with CO_2-emission-neutral electricity, the substitution of natural gas with hydrogen and synthetic methane results in considerable emission savings in the steel mill and in the higher-level energy system. Depending on the system configuration, the absolute emission reduction corresponds to 40–50% of the scope 1 CO_2 emissions of the steel mill.

Q 3. *Which economic framework conditions are required for their economically viable operation?*

Low electricity prices and specific investment costs favor the use of power-to-gas technologies. Furthermore, increasing emission allowance prices are decisive for the substitution of natural gas by green gases such as hydrogen or SNG. In their long-term strategy for a climate-neutral economy [59], the European Commission emphasizes the relevance of the ETS in achieving its climate goals. As demonstrated in our study, emission allowance

prices serve as a price signal that triggers investments in climate-neutral technologies. For an emission reduction between 80 and 100%, carbon dioxide prices in the range of 250 to 350 EUR/t$_{CO2}$ are expected by 2050. Hence, the decreasing specific capital expenditures, the increase in situations with extremely low electricity prices, and the expected surge of emission certificate prices towards the year 2050 make PEM electrolysis not only a viable flexibility option for the future electricity grid but also an effective enabler for a climate-neutral energy system.

Author Contributions: Conceptualization, J.D. and T.K.; methodology, J.D. and T.K.; software, S.W.; validation, J.D.; formal analysis, J.D., S.W. and A.T.; investigation, J.D. and S.W.; resources, J.D.; data curation, J.D., S.W. and A.T.; writing—original draft preparation, J.D., T.K. and A.T.; writing—review and editing, T.K.; visualization, J.D.; supervision, T.K.; project administration, J.D.; funding acquisition, T.K. All authors have read and agreed to the published version of the manuscript.

Institutional Review Board Statement: Not applicable.

Informed Consent Statement: Not applicable.

Data Availability Statement: Not applicable.

Conflicts of Interest: The authors declare no conflict of interest.

References

1. Material Economics. Industrial Transformation 2050—Pathways to Net-Zero Emissions from EU Heavy Industry. 2019. Available online: https://materialeconomics.com/publications/industrial-transformation-2050 (accessed on 21 October 2021).
2. International Energy Agency. Iron and Steel Technology Roadmap, Paris. 2020. Available online: https://www.iea.org/reports/iron-and-steel-technology-roadmap (accessed on 22 October 2021).
3. The Boston Consulting Group (BCG), Steel Institute VDEh. Steel's Contribution to a Low-Carbon Europe 2050: Technical and Economic Analysis of the Sector's CO2 Abatement Potential. 2013. Available online: https://www.bcg.com/publications/2013/metals-mining-environment-steels-contribution-low-carbon-europe-2050 (accessed on 13 January 2022).
4. ICF Consulting Services Limited, Fraunhofer Institute for Systems and Innovation Research. Industrial Innovation: Pathways to Deep Decarbonisation of Industry: Part 2: Scenario Analysis and Pathways to Deep Decarbonisation. 2019. Available online: https://www.isi.fraunhofer.de/de/competence-center/energietechnologien-energiesysteme/projekte/pathways.html#3 (accessed on 28 October 2021).
5. World Resources Institute, World Business Council for Sustainable Development. The Greenhouse Gas Protocol. Available online: https://ghgprotocol.org/standards (accessed on 19 November 2021).
6. Dock, J.; Kienberger, T. Techno-economic case study on Oxyfuel technology implementation in EAF steel mills—Concepts for waste heat recovery and carbon dioxide utilization. *Clean. Eng. Technol.* **2022**, *9*, 100525. [CrossRef]
7. Bussar, C.; Stöcker, P.; Cai, Z.; Moraes Jr., L.; Magnor, D.; Wiernes, P.; van Bracht, N.; Moser, A.; Sauer, D.U. Large-scale integration of renewable energies and impact on storage demand in a European renewable power system of 2050—Sensitivity study. *J. Energy Storage* **2016**, *6*, 1–10. [CrossRef]
8. Greiml, M.; Fritz, F.; Kienberger, T. Increasing installable photovoltaic power by implementing power-to-gas as electricity grid relief—A techno-economic assessment. *Energy* **2021**, *235*, 121307. [CrossRef]
9. Dock, J.; Janz, D.; Weiss, J.; Marschnig, A.; Kienberger, T. Time- and component-resolved energy system model of an electric steel mill. *Clean. Eng. Technol.* **2021**, *4*, 100223. [CrossRef]
10. Madias, J. Electric furnace steelmaking. In *Treatise on Process Metallurgy*; Elsevier: Kidlington, Oxford, UK; Waltham, MA, USA, 2014; pp. 271–300. ISBN 978-0-08-096988-6.
11. Holappa, L. Secondary steelmaking. In *Treatise on Process Metallurgy*; Elsevier: Kidlington, Oxford, UK; Waltham, MA, USA, 2014; pp. 301–345. ISBN 978-0-08-096988-6.
12. Warren, P. A review of demand-side management policy in the UK. *Renew. Sustain. Energy Rev.* **2014**, *29*, 941–951. [CrossRef]
13. Paulus, M.; Borggrefe, F. The potential of demand-side management in energy-intensive industries for electricity markets in Germany. *Appl. Energy* **2011**, *88*, 432–441. [CrossRef]
14. Strbac, G. Demand side management: Benefits and challenges. *Energy Policy* **2008**, *36*, 4419–4426. [CrossRef]
15. Marchiori, F.; Belloni, A.; Benini, M.; Cateni, S.; Colla, V.; Ebel, A.; Lupinelli, M.; Nastasi, G.; Neuer, M.; Pietrosanti, C.; et al. Integrated dynamic energy management for steel production. *Energy Procedia* **2017**, *105*, 2772–2777. [CrossRef]
16. Zhang, Q.; Grossmann, I.E. Enterprise-wide optimization for industrial demand side management: Fundamentals, advances, and perspectives. *Chem. Eng. Res. Des.* **2016**, *116*, 114–131. [CrossRef]

17. Gorre, J.; Ortloff, F.; van Leeuwen, C. Production costs for synthetic methane in 2030 and 2050 of an optimized Power-to-Gas plant with intermediate hydrogen storage. *Appl. Energy* **2019**, *253*, 113594. [CrossRef]

18. Kato, T.; Kubota, M.; Kobayashi, N.; Suzuoki, Y. Effective utilization of by-product oxygen from electrolysis hydrogen production. *Energy* **2005**, *30*, 2580–2595. [CrossRef]

19. McGuinness, R.M.; Kleinberg, W.T. Oxygen production. In *Oxygen-Enhanced Combustion*, 2nd ed.; Baukal, C.E., Ed.; CRC Press: Boca Raton, FL, USA, 2013; pp. 44–74. ISBN 978-1-4398-6230-8.

20. Kerry, F.G. Noncryogenic oxygen production. In *Oxygen-Enhanced Combustion*, 2nd ed.; Baukal, C.E., Ed.; CRC Press: Boca Raton, FL, USA, 2013; pp. 77–87. ISBN 978-1-4398-6230-8.

21. Šulc, R.; Ditl, P. A technical and economic evaluation of two different oxygen sources for a small oxy-combustion unit. *J. Clean. Prod.* **2021**, *309*, 127427. [CrossRef]

22. Air Liquide Engineering and Construction. Standard Plants: Fully Packaged Modular Solutions. Available online: https://www.engineering-airliquide.com/standard-plants (accessed on 7 January 2022).

23. PCI Oxygen Solutions. On-Site Oxygen Solutions: Industrial. Available online: https://www.pcigases.com/oxygen-solutions/marketing-literature/ (accessed on 7 January 2022).

24. Adsorptech. EcoGen™ Oxygen VPSA Onsite Generator. Available online: https://adsorptech.com/wp-content/uploads/2021 Adsorptech-EcoGen-2111-2.pdf (accessed on 7 January 2022).

25. Banaszkiewicz, T.; Chorowski, M.; Gizicki, W. Comparative analysis of oxygen production for oxy-combustion application. *Energy Procedia* **2014**, *51*, 127–134. [CrossRef]

26. Bailera, M.; Kezibri, N.; Romeo, L.M.; Espatolero, S.; Lisbona, P.; Bouallou, C. Future applications of hydrogen production and CO_2 utilization for energy storage: Hybrid power to gas-oxycombustion power plants. *Int. J. Hydrogen Energy* **2017**, *42*, 13625–13632. [CrossRef]

27. Schiebahn, S.; Grube, T.; Robinius, M.; Tietze, V.; Kumar, B.; Stolten, D. Power to gas: Technological overview, systems analysis and economic assessment for a case study in Germany. *Int. J. Hydrogen Energy* **2015**, *40*, 4285–4294. [CrossRef]

28. Mergel, J.; Carmo, M.; Fritz, D. Status on technologies for hydrogen production by water electrolysis. In *Transition to Renewable Energy Systems*; Wiley-VCH: Weinheim, Germany, 2013; pp. 425–450. ISBN 978-3-527-33239-7.

29. Schmidt, O.; Gambhir, A.; Staffell, I.; Hawkes, A.; Nelson, J.; Few, S. Future cost and performance of water electrolysis: An expert elicitation study. *Int. J. Hydrogen Energy* **2017**, *42*, 30470–30492. [CrossRef]

30. Iora, P.; Chiesa, P. High efficiency process for the production of pure oxygen based on solid oxide fuel cell–solid oxide electrolyzer technology. *J. Power Sources* **2009**, *190*, 408–416. [CrossRef]

31. Iora, P.; Taher, M.A.A.; Chiesa, P.; Brandon, N.P. A one dimensional solid oxide electrolyzer-fuel cell stack model and its application to the analysis of a high efficiency system for oxygen production. *Chem. Eng. Sci.* **2012**, *80*, 293–305. [CrossRef]

32. Ghaib, K.; Nitz, K.; Ben-Fares, F.-Z. Chemical methanation of CO_2: A review. *ChemBioEng Rev.* **2016**, *3*, 266–275. [CrossRef]

33. Herrmann, F.; Grünewald, M.; Meijer, T.; Gardemann, U.; Feierabend, L.; Riese, J. Operating window and flexibility of a lab-scale methanation plant. *Chem. Eng. Sci.* **2022**, *254*, 117632. [CrossRef]

34. Chwoła, T.; Spietz, T.; Więcław-Solny, L.; Tatarczuk, A.; Krótki, A.; Dobras, S.; Wilk, A.; Tchórz, J.; Stec, M.; Zdeb, J. Pilot plant initial results for the methanation process using CO_2 from amine scrubbing at the Łaziska power plant in Poland. *Fuel* **2020**, *263*, 116804. [CrossRef]

35. Gorre, J.; Ruoss, F.; Karjunen, H.; Schaffert, J.; Tynjälä, T. Cost benefits of optimizing hydrogen storage and methanation capacities for Power-to-Gas plants in dynamic operation. *Appl. Energy* **2020**, *257*, 113967. [CrossRef]

36. Van Rossum, G. The Python Library Reference. Release 3.7.8rc1. 2020. Available online: https://docs.python.org/3.7/library/index.html (accessed on 24 June 2020).

37. Hilpert, S.; Kaldemeyer, C.; Krien, U.; Günther, S.; Wingenbach, C.; Plessmann, G. The open energy modelling framework (oemof)—A new approach to facilitate open science in energy system modelling. *Energy Strategy Rev.* **2018**, *22*, 16–25. [CrossRef]

38. Krien, U.; Schönfeldt, P.; Launer, J.; Hilpert, S.; Kaldemeyer, C.; Pleßmann, G. Oemof.solph—A model generator for linear and mixed-integer linear optimisation of energy systems. *Softw. Impacts* **2020**, *6*, 100028. [CrossRef]

39. Buttler, A.; Spliethoff, H. Current status of water electrolysis for energy storage, grid balancing and sector coupling via power-to-gas and power-to-liquids: A review. *Renew. Sustain. Energy Rev.* **2018**, *82*, 2440–2454. [CrossRef]

40. Carmo, M.; Fritz, D.L.; Mergel, J.; Stolten, D. A comprehensive review on PEM water electrolysis. *Int. J. Hydrogen Energy* **2013**, *38*, 4901–4934. [CrossRef]

41. International Energy Agency. The Future of Hydrogen: Seizing Today's Opportunities, Paris. 2019. Available online: https://www.iea.org/reports/the-future-of-hydrogen (accessed on 3 January 2022).

42. Mutz, B.; Carvalho, H.W.P.; Mangold, S.; Kleist, W.; Grunwaldt, J.-D. Methanation of CO_2: Structural response of a Ni-based catalyst under fluctuating reaction conditions unraveled by operando spectroscopy. *J. Catal.* **2015**, *327*, 48–53. [CrossRef]

43. Energy Brainpool. Trends in the Development of Electricity Prices—EU Energy Outlook 2050. Available online: https://blog.energybrainpool.com/en/trends-in-the-development-of-electricity-prices-eu-energy-outlook-2050/ (accessed on 16 February 2022).

44. Energy Brainpool. Update: EU Energy Outlook 2050—How will Europe Evolve over the Next 30 Years? Available online: https://blog.energybrainpool.com/en/update-eu-energy-outlook-2050-how-will-europe-evolve-over-the-next-30-years/ (accessed on 16 February 2022).

45. van Leeuwen, C.; Mulder, M. Power-to-gas in electricity markets dominated by renewables. *Appl. Energy* **2018**, *232*, 258–272. [CrossRef]

46. E4tech, E.E. Development of Water Electrolysis in the European Union: Final Report. 2014. Available online: https://www.fch.europa.eu/node/783 (accessed on 20 December 2021).

47. Peters, M.S.; Timmerhaus, K.D.; West, R.E. *Plant Design and Economics for Chemical Engineers*, 5th ed.; McGraw-Hill: Boston, MA, USA, 2004; ISBN 0-07-239266-5.

48. Austrian Power Grid AG. EXAA Day-Ahead Prices 2020. Available online: https://www.apg.at/de/markt/Markttransparenz/Uebertragung/EXAA-Spotmarkt (accessed on 21 December 2021).

49. Traupmann, A.; Greiml, M.; Steinegger, J.; Kühberger, L.; Kienberger, T. Sector coupling technologies as re-purposing options for coal-fired power plants in the austrian grids—A MES approach. *Sustain. Energy Technol. Assess.* 2022; *under review*.

50. International Energy Agency. World Energy Outlook 2021, Paris. 2021. Available online: https://www.iea.org/reports/world-energy-outlook-2021 (accessed on 4 January 2022).

51. European Energy Exchange AG. Emission Spot Primary Market Auction Report 2020. Available online: https://www.eex.com/en/market-data/environmental-markets/eua-primary-auction-spot-download (accessed on 21 December 2021).

52. Pietzcker, R.C.; Osorio, S.; Rodrigues, R. Tightening EU ETS targets in line with the European Green Deal: Impacts on the decarbonization of the EU power sector. *Appl. Energy* **2021**, *293*, 116914. [CrossRef]

53. Cvetkovska, R.; Nagovnak, P.; Kienberger, T. Pathways for ramping-up hydrogen into the natural gas system. In Proceedings of the 17th Symposium Eneergieinnovation, Future of Energy: Innovationen für Eine Klimaneutrale Zukunft, Graz, Austria, 16–18 February 2022.

54. Gas-Systemnutzungsentgelte-Verordnung. Available online: https://www.ris.bka.gv.at/GeltendeFassung.wxe?Abfrage=Bundesnormen&Gesetzesnummer=20007992&FassungVom=2022-06-02 (accessed on 28 June 2022).

55. E-Control. Natural Gas: Taxes and Surcharges. Available online: https://www.e-control.at/en/industrie/gas/gaspreis/steuern-und-abgaben (accessed on 28 June 2022).

56. Systemnutzungsentgelte-Verordnung 2018. Available online: https://www.ris.bka.gv.at/GeltendeFassung.wxe?Abfrage=Bundesnormen&Gesetzesnummer=20010107&FassungVom=2022-01-01 (accessed on 28 June 2022).

57. E-Control. Electricity: Taxes and Surcharges. Available online: https://www.e-control.at/en/industrie/strom/strompreis/steuern (accessed on 28 June 2022).

58. Electricity Industry and Organization Act: ElWOG. 2010. Available online: https://www.ris.bka.gv.at/GeltendeFassung.wxe?Abfrage=Bundesnormen&Gesetzesnummer=20007045 (accessed on 5 April 2022).

59. European Commission. A Clean Planet for All—A European Long-Term Strategic Vision for a Prosperous, Modern, Competitive and Climate Neutral Economy: In-Depth Analysis in Support of the Commission Communication COM (2018) 773, 28th 2018. Available online: https://ec.europa.eu/clima/eu-action/climate-strategies-targets/2050-long-term-strategy_en (accessed on 30 June 2022).